Article

Study of Radiation Damage Kinetics in Dispersed Nuclear Fuel on Zirconium Dioxide Doped with Cerium Dioxide

Artem L. Kozlovskiy [1,2,3,*], Daryn B. Borgekov [1,3], Maxim V. Zdorovets [1,3], Inesh E. Kenzhina [2,3,4] and Dmitriy I. Shlimas [1,3]

1   Engineering Profile Laboratory, L.N. Gumilyov Eurasian National University, Astana 010008, Kazakhstan; borgekov@mail.ru (D.B.B.); mzdorovets@gmail.com (M.V.Z.)
2   Department of General Physics, Satbayev University, Almaty 050032, Kazakhstan; kenzhina@physics.kz
3   Laboratory of Solid State Physics, The Institute of Nuclear Physics, Almaty 050032, Kazakhstan
4   Advanced Electronics Development Laboratory, Kazakh-British Technical University, 59 Tole bi St., Almaty 050000, Kazakhstan
*   Correspondence: kozlovskiy.a@inp.kz; Tel./Fax: +7-7024413368

Abstract: One area that holds promise for nuclear energy advancement, which is the most attractive industry for eliminating the imbalance in the energy sector and reducing the world's energy shortage for the long term, is the replacement of traditional uranium fuel with plutonium fuel. The focus on this research area is due to the growing concern of the world community about the problem of handling spent nuclear fuel, including its further use or storage and disposal. The main aims of this paper are to study the resistance of composite ceramics based on zirconium and cerium dioxide to the hydrogenation processes and subsequent destructive embrittlement, and to identify patterns of growth stability attributable to the occurrence of interfacial boundaries and changes in the phase composition of ceramics. Studies have shown that the main effects of the structural distortion of the crystalline structure of ceramics are caused primarily by tensile deformation distortions, resulting in the accumulation of radiation-induced damage. The formation of $Zr_{0.85}Ce_{0.15}O_2$ tetragonal phase of replacement in the structure of ceramics results in a more than two-fold reduction in the deformation distortion degree in cases of high-dose radiation with protons. The evaluation of the alteration in the strength properties of ceramics revealed that the variation in the phase composition due to polymorphic transformation of the monoclinic $Zr_{0.98}Ce_{0.02}O_2 \rightarrow$ tetragonal $Zr_{0.85}Ce_{0.15}O_2$ type results in the strengthening of the damaged layers and the improvement of the resistance to radiation-induced embrittlement and softening.

Keywords: structural ceramics; radiation embrittlement; hydrogen swelling; zirconium dioxide; radiation damage resistance

1. Introduction

In view of recent worldwide trends in the advancement of the energy sector, alongside the transition from hydrocarbons to alternative energy sources, much attention has been paid to nuclear energy as well as its development towards the creation of new nuclear reactor types and the search for opportunities to increase productivity and increase the life of existing nuclear power plants. Much attention has been paid to the transition from traditional uranium dioxide-based (UO_2) fuel assemblies to dispersed nuclear fuel with the aim of improving productivity and service life [1–3]. In the transition of nuclear reactors to dispersed nuclear fuel, with the possibility of processing weapons-grade plutonium and reducing the accumulation of long-lived nuclear waste, some of the most promising materials are composite ceramics of the cer–cer type, consisting of refractory oxide, nitride or carbide compounds [4,5]. The focus on these types of ceramics has increased primarily as the use of refractory oxides, nitrides and carbides as materials of inert nuclear fuel matrices will allow the isolation of fissile material particles from each other; in addition,

due to high radiation resistance and mechanical strength, it is possible to increase the life and burnup degree of nuclear fuel, which will increase its operating time [6,7]. The use of refractory oxide compounds allows the increase in the temperature conditions of operation, and small thermal expansion coefficient values of materials such as zirconium dioxide (ZrO_2), cerium dioxide (CeO_2) and magnesium oxide (MgO) make it possible to exclude the effect of a rise in the volume of the ceramic crystal structure, which may adversely affect the properties of the material, as well as exert additional pressure on the fissile and inert matrix materials [8–10]. An important factor in the study of ceramic materials that could potentially be used as nuclear structural materials is the study of their effects associated with the accumulation of radiation-induced damage, arising from various types of ionizing radiation, including neutron exposure, which has a high penetrating ability [11–13]. It has been shown in several works that, despite its nature (charge-neutrality) and small size, neutron irradiation can result in deformation distortions, processes associated with embrittlement and a decrease in strength properties. At the same time, in contrast to heavy ions, the thickness of the damaged layers during neutron irradiation is much larger, which is associated with the high penetrating power of neutrons, and the defects arising from them can result in catastrophic consequences, leading to the destabilization of materials [14–17].

However, despite the excellent prospects in this area of research, there are still many issues concerning the problem of radiation swelling of the surface layer, which due to the cumulative effect can result in the partial destruction and deformation of the surface of the inert matrix that is in contact with the fissile material, thereby violating the thermal insulation properties of the ceramics [18–20]. With the radiation damage accumulation in the near-surface layer, structurally disordered or amorphous regions may appear. This is accompanied by a rise in the deformation distortions of the structure, which create additional mechanical stresses in the damaged layers [21–23]. When it comes to the accumulation of hydrogen or helium, their nature allows them to agglomerate in voids or deformed areas with a subsequent increase in volume, causing the occurrence of tensile deformation stresses [24–26]. In this regard, the study of the mechanisms of radiation-induced swelling represents very important research [27,28] alongside the search for ways to combat this issue via the alteration of the components' composition, grain sizes, boundary, and interfacial effects [29,30].

The aim of this work is to investigate the effectiveness of the influence of the cerium dioxide dopant concentration on the stability of dispersed nuclear fuel based on zirconium dioxide in terms of the accumulation of radiation-induced damage in the near-surface layer of the ceramics. The irradiation of ceramics was conducted via proton radiation in order to determine the mechanisms associated with the swelling processes during implanted hydrogen agglomeration and the consequences arising from swelling.

As objects for research, dispersed fuel was chosen in conformity with the type of cer–cer (ceramic–ceramic) compositions based on zircaloy ceramics doped with cerium dioxide [31–33]. These materials were chosen due to their high thermal expansion resistance, mechanical strength and thermal resistance, alongside a high degree of compatibility with different structural materials. This makes it possible to use them in various compositions in the development of dispersed fuel, as well as enabling the replacement of traditional fuel elements with uranium dioxide for uranium-free fuel. X-ray diffraction and transmission electron microscopy were chosen as the main research methods for assessing radiation damage in this work. These are high-precision, non-destructive control methods that make it possible to determine the kinetics of accumulation of radiation damage with high accuracy as well as establishing the main causes associated with deformation distortions of the structure [34,35]. Thus, in a number of works [36,37] using high-resolution electron microscopy, the results of the relationship between the latent tracks formed as a result of irradiation, mechanical residual stresses, structural changes and amorphization processes were obtained. Using the X-ray diffraction analysis aimed at assessing alterations in structural parameters and their distortion, dose dependences of the crystal lattice swelling and its deformation as a function of the irradiation fluence were obtained in a number of

works [38,39]. At the same time, the established dependences make it possible to evaluate the resistance of materials to the processes of radiation damage, alongside the kinetics of their occurrence, which in the future will make it possible to predict the behavior of structural materials exposed to ionizing radiation.

2. Experimental Part

Ceramics of the cer–cer type obtained by mechanochemical solid-phase synthesis followed by thermal sintering at 1500 °C were chosen as specimens for this research. Zirconium (ZrO_2) and cerium (CeO_2) oxides were chosen as initial components for the synthesis of cer–cer ceramics; the compounds' chemical purity was 99.95%. Powders were acquired from Sigma Aldrich (Sigma, St. Louis, MI, USA). The mechanochemical synthesis was carried out by mixing these oxides in the selected molar ratio, followed by grinding in a PULVERISETTE 6 classic line planetary mill (Fritsch, Idar-Oberstein, Germany) at a speed of 400 rpm for 60 min. After grinding, the obtained specimens were pressed into pellets 10 mm in diameter and 50 µm thick and subjected to high-temperature annealing in a SNOL muffle furnace (SNOL-TERM, St. Petersburg, Russia) at 1500 °C for 8 h. After annealing, the samples were cooled to room temperature for 24 h together with the furnace.

The irradiation of the samples to determine the radiation resistance to superhydrogenation and subsequent embrittlement was carried out at the UKP-2 accelerator. For irradiation, protons with an energy of 1.0 MeV and irradiation fluences of 10^{14}–10^{17} proton/cm^2 were chosen. The highest run length for protons with an energy of 1.0 MeV in ceramics is more than 10 µm. In conformity with theoretical estimates via the SRIM Pro 2013 program code, the ionization losses of incident protons throughout interaction with electron shells ($dE/dx_{electron}$) are 0.2 keV/nm and with nuclei ($dE/dx_{nuclear}$) are 0.00013 keV/nm. A values of 25 eV was chosen as the threshold displacement energy. The choice of irradiation fluences corresponds to the dpa values of ~0.01–10 dpa, which in turn makes it possible to estimate the hydrogenation mechanisms and their effect on the structural distortion of ceramics throughout accumulation of structurally distorted regions in the damaged near-surface layer. Moreover, the calculated data showed that at the highest irradiation fluence, the concentration of implanted protons at the maximum path length is no more than 1.5 at.%. Thus, we can conclude that the main contribution to the alteration in the features of ceramics under high-dose irradiation will come from both structural distortions arising from the accumulation of atomic displacements and the effects associated with the accumulation of implanted hydrogen in the voids of the crystal lattice.

The study of the structural features of the obtained ceramics as a function of the concentration of the CeO_2 dopant in the composition of ceramics, alongside the processes of phase transformations related to an alteration in the concentration of the dopant, was carried out using the X-ray phase analysis method. This method was implemented using a D8 Advance ECO X-ray diffractometer (Bruker, Berlin, Germany). Obtaining X-ray diffraction patterns was carried out in the Bragg–Brentano geometry, in the angular range 2θ = 20–90°, scanning step 0.03°. The obtained diffraction patterns were deciphered in the DiffracEVA v.4.2 program code, the phase composition was ascertained via card values from the PDF-2 (2016) database.

The study of deformation structural distortions of the crystal lattice was carried out via a comparative analysis of changes in the parameters of the samples before and after irradiation, considering a priori information about the initial values of the parameters and volume of the crystal lattice of the samples in the initial state.

To analyze the morphological features of the obtained ceramics, as well as to establish the presence of defective or amorphous inclusions in the grains, high-resolution transmission electron microscopy was used. Images for further analysis were obtained using a Jeol JEM-1400Plus transmission electron microscope (Jeol, Tokyo, Japan).

The study of the hardness of ceramics as a function of the dopant concentration, as well as the irradiation fluence variation and the resulting accumulated radiation-induced damage in the near-surface layer, was carried out using the microindentation technique. To

obtain hardness values, a LECO LM700 microhardness tester (LECO, Tokyo, Japan) was used. The hardness analysis was carried out considering the geometry of the indenter (Vickers pyramid), alongside the load on the indenter, which was 1 kN. To collect statistics, all measurements were performed in a successive series (20–25 measurements), considering the possibility of avoiding contact of the indenter prints during the measurement. To achieve this, after each measurement, the indenter was moved to several microns from the previous measurement site. The determination of the values of softening and embrittlement of ceramics as a function of the irradiation fluence was carried out via comparative analysis of the obtained hardness values of the irradiated samples with the initial values (the original non-irradiated sample). The dependences obtained made it possible to determine how efficient the CeO_2 dopant effect is on the increase in hardness and crack resistance, as well as on the change in resistance to destructive embrittlement and softening with a rise in the concentration of accumulated damage.

3. Results and Discussion

3.1. Characterization of Initial Samples as a Function of the Variation of CeO_2 Dopant Concentration

Figure 1 illustrates the X-ray phase analysis results of the synthesized ceramics of the cer–cer type with different variations of the CeO_2 dopant. The general dynamics of the changes in X-ray diffraction patterns as a function of the concentration of the CeO_2 dopant indicates that there are phase transformations arising from doping, accompanied by partial replacement of zirconium atoms by cerium atoms. At low concentrations of the CeO_2 dopant (0.05 mol), the ceramic samples represent a ZrO_2 monoclinic phase, which is characteristic of zirconium ceramics obtained by the solid-phase synthesis from powders. In this case, no polymorphic transformations associated with the transformation of the monoclinic phase into a tetragonal or cubic phase were observed under the chosen synthesis conditions, which is in good agreement with several datasets from the literature [40–42]. When the CeO_2 dopant concentration increases to 0.10 mol, in conformity with the data of the X-ray phase analysis, the transformation of the ZrO_2 phase into the $Zr_{0.98}Ce_{0.02}O_2$ phase is observed with the preservation of the monoclinic crystal lattice type. Such a phase transformation is associated with the effect of the partial substitution of zirconium atoms by cerium atoms in the crystal lattice, since for these oxides there are quite a lot of substitution phases with different concentrations of substituted atoms [43,44]. With a growth in the concentration of the CeO_2 dopant to 0.15 mol, the formation of polymorphic phase transformations in the composition of ceramics is observed with the formation of a $Zr_{0.85}Ce_{0.15}O_2$ phase with a tetragonal crystal lattice type; the formation of which occurs by the phase rearrangement of the $Zr_{0.98}Ce_{0.02}O_2$ monoclinic phase into the tetragonal $Zr_{0.85}Ce_{0.15}O_2$ with a rise in the effect of substitution of zirconium for cerium. Such polymorphic phase transformations are typical for the structure of zirconia ceramics when magnesium [45], yttrium [46] or calcium [47,48] oxides are added to it, which results in the initialization of polymorphic transformation processes at lower temperatures (1300–1500 °C), at which no polymorphic transformations are observed in the case of pure zirconia [49].

In conformity with the X-ray phase analysis data, an alteration in the CeO_2 dopant concentration results in the initialization of phase transformation processes, which can be written as follows: monoclinic $ZrO_2 \rightarrow$ monoclinic $Zr_{0.98}Ce_{0.02}O_2 \rightarrow$ tetragonal $Zr_{0.85}Ce_{0.15}O_2$. The formation of the $Zr_{0.85}Ce_{0.15}O_2$ tetragonal phase occurs at CeO_2 concentrations of more than 0.15 mol, and is associated with polymorphic transformations of zirconium dioxide, which are typical for cases when dopant concentrations exceed a certain threshold value and result in the initialization of phase transformation processes. In the case of magnesium dioxide, the limiting threshold value for phase polymorphic transformations is 0.03–0.10 mol [50], and in the case of cerium dioxide, in conformity with the data obtained, the initialization of polymorphic transformations occurs at a CeO_2 dopant concentration of 0.15 mol, and at a concentration of 0.25, a complete polymorphic transformation of the monoclinic $Zr_{0.98}Ce_{0.02}O_2 \rightarrow$ tetragonal $Zr_{0.85}Ce_{0.15}O_2$ type occurs.
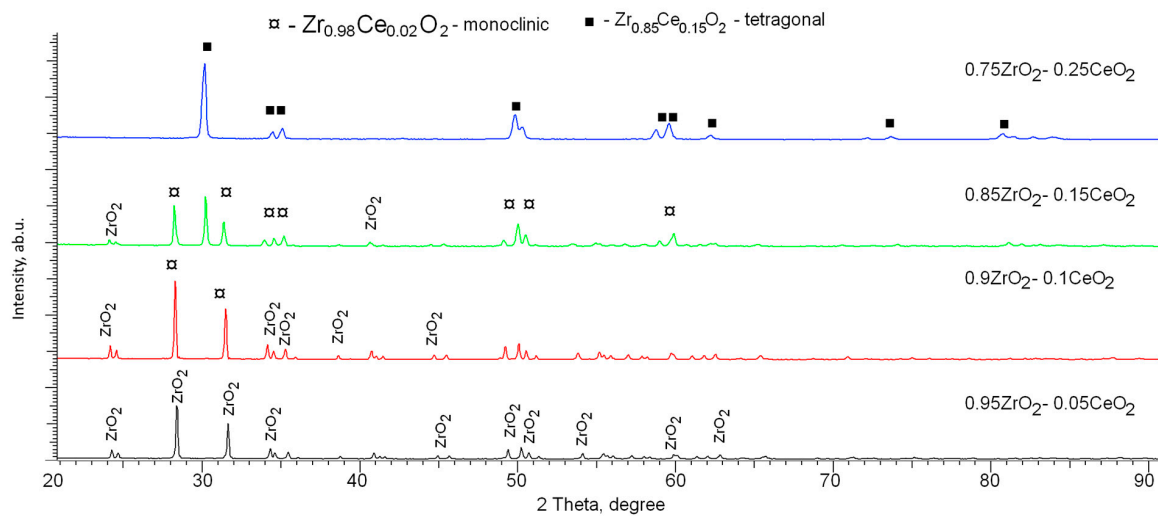
Figure 1. X-ray diffraction patterns of the investigated samples of ceramics in the initial state.

Figure 2 demonstrates the results of phase transformations in ceramics performed using the transmission electron microscopy method; it is clearly seen that the formation of tetragonal inclusions occurs in the form of grains, which subsequently, at a high concentration of the CeO_2 dopant, result in a complete transformation of ceramic particles. In that case, the tetragonal phase formation occurs when smaller particles coalesce into large agglomerates with the formation of $Zr_{0.85}Ce_{0.15}O_2$ particles within them, and a rise in the concentration results in the complete transformation of the monoclinic phase into a tetragonal one. Moreover, grain coarsening is accompanied by elevation in the degree of structural ordering, the results of which are presented in Table 1.
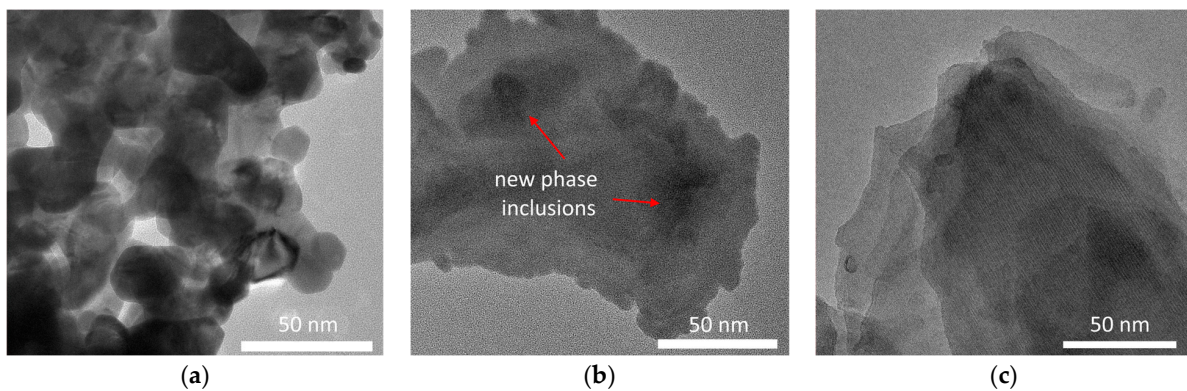

Figure 2. TEM images of synthesized ceramics after thermal annealing (1500 °C) with various concentrations of CeO_2 dopant: (**a**) 0.05 mol; (**b**) 0.15 mol; (**c**) 0.25 mol.

Table 1. Structural analysis data of the obtained ceramic samples as a function of the CeO_2 concentration.

Parameter	CeO_2 Concentration, mol			
	0.05	0.10	0.15	0.25
Degree of structural ordering (crystallinity degree *), %	88.4 ± 0.3	89.3 ± 0.2	92.2 ± 0.7	94.7 ± 0.5
Deformation factor of crystal lattice distortion **	0.023 ± 0.005	0.021 ± 0.005	0.028 ± 0.006	0.019 ± 0.004

* The degree of structural ordering (degree of crystallinity) is determined by a comparative analysis of the contributions from the areas of diffraction reflections and background radiation, characteristic of a disordered or amorphous structure. ** The deformation factor of the crystal lattice distortion is estimated from the alteration in the crystal lattice parameters in comparison with their deviation from the reference values.

As is evident from the data on changes in the degree of structural ordering (degree of crystallinity), the formation of processes of polymorphic transformations of the monoclinic $Zr_{0.98}Ce_{0.02}O_2 \rightarrow$ tetragonal $Zr_{0.85}Ce_{0.15}O_2$ type is accompanied by a decrease in the contribution of background radiation (the concentration of disordered regions and amorphous inclusions), which indicates the formation of structurally ordered ceramics with a high crystallinity degree. Moreover, the deformation factor analysis of the crystal lattice distortion has a pronounced dependence on the formation of the $Zr_{0.85}Ce_{0.15}O_2$ tetragonal phase in the ceramic structure, the appearance of which in the composition of ceramics results in a growth in crystal lattice distortion due to the occurrence of interphase boundaries that contribute to the formation of deformation distortions. Moreover, in the case of a complete polymorphic transformation and subsequent shift of the monoclinic phase from the composition of ceramics, a decrease in the deformation distortion of the crystal lattice is observed.

Therefore, analyzing the data acquired, we can assume that the CeO_2 dopant concentration growth from 0.05 to 0.025 mol results in the formation of a stable tetragonal $Zr_{0.85}Ce_{0.15}O_2$ substitution phase, which has a high structural ordering degree and a low deformation distortion of the crystal structure.

3.2. Study of the Kinetics of Deformation Distortion of the Crystal Structure of Ceramics as a Function of Dopant Concentration under High-Dose Proton Irradiation

One of the important criteria for the applicability of composite ceramics as materials for the creation of dispersed nuclear fuel is their resistance to radiation-induced damage, alongside the processes accompanied by the accumulation of these damages in the damaged layers. One of the key problems in this direction is resistance to hydrogenation and subsequent embrittlement as a result of the formation of structurally distorted regions and gas-filled inclusions. The resistance of materials to hydrogenation and subsequent destruction can be assessed using the method of X-ray diffraction analysis by calculating the dynamics of changes in structural parameters, in particular the deformation factor of crystal lattice distortion, as well as changes in the degree of structural ordering (degree of crystallinity). Having determined the dynamics of changes in these structural parameters as a function of the irradiation fluence or the value of atomic displacements arising from irradiation, it is possible to establish the criteria for the applicability of these ceramics as materials for dispersed nuclear fuel.

Figure 3 illustrates the assessment results of the degree of structural disorder arising from the crystal lattice deformation distortion of the synthesized ceramics as a function of the concentration of the cerium dioxide dopant component in the composition of the ceramics. The dependences obtained were calculated on the basis of data on the assessment of the alteration in the crystal lattice parameters as a function of the proton irradiation fluence when estimating the position of diffraction reflections in diffraction patterns. The overall appearance of the presented trend in the alteration in the deformation distortion of the crystal structure indicates the tensile nature of structural distortions associated with the accumulation of radiation-induced damage in the composition of ceramics, alongside the deformation distortion of the crystal structure during high-dose irradiation, which is characteristic of partial amorphization.

The general trends of the alteration in the degree of crystal lattice deformation indicate a two-stage nature of the change in deformation distortions. The first stage consists of the accumulation of point defects arising from irradiation, which, in conformity with the assessment of the degree of deformation, results in small changes in the parameters of the crystal lattice. In this case, the main structural changes associated with the formation of tensile deformation distortions are attributable to ionization processes and subsequent changes in the electron density and its distribution. Ionization occurs during the interaction of projectile particles with the electronic subsystem of ceramics, which results in the formation of cascade effects of secondary electrons capable of migrating to a sufficiently large distance from the main trajectory of projectile particles [51,52]. With a high

irradiation fluence, the number of ionization events is quite large, which results in the formation of overlapping effects of such areas, and as a result, the appearance of structural distortions arising from ionization. Moreover, these effects of structural distortions are cumulative. Upon reaching the critical point, the deformation of the crystal lattice sharply increases, which indicates the effect of disordering and partial destruction associated with amorphization or hydrogenation processes. The critical point for increasing structural distortions associated with the accumulation of tensile strains is the irradiation fluence of 10^{15}–5×10^{15} cm^{-2}; upon reaching this, a sharp increase in the deformation distortion of the crystal structure is observed [53,54]. One must note that at these irradiation fluences, there are also differences in the magnitude of the structural distortion of the crystal lattice for samples with a tetragonal type of crystal structure $Zr_{0.85}Ce_{0.15}O_2$. In the case of a tetragonal structure of ceramics at a CeO_2 dopant concentration of 0.25 mol, the deformation distortion of the crystal structure at the maximum irradiation fluence is less than 10%, which is more than two times less than the results of the other samples. This difference can be explained by the fact that in the case of a monoclinic structure, which is characteristic of the ZrO_2 and $Zr_{0.98}Ce_{0.02}O_2$ phases, deformation distortions occur more intensely. Since it is known that during irradiation of ceramics with a ZrO_2 monoclinic phase at high irradiation fluences, polymorphic transformation processes occur, arising from the deformation distortion accumulation [55–57]. However, when it comes to proton irradiation, the values of ionization losses are much smaller than in the case of irradiation of heavy ions [55–57], which in turn results in the formation of a large number of deformation distortions, but is not sufficient to initiate the processes of polymorphic transformations of the m-$ZrO_2 \rightarrow$ t-ZrO_2 type [55–57], which are characteristic of irradiation with heavy ions. In this case, it can be concluded that ceramics with a monoclinic type of crystal lattice are less resistant to deformation distortions arising from ionization processes, since the structure of ceramics itself is a metastable state, which changes under any external influences, including ionization effects and a change in the electron density. It should also be noted that, in conformity with calculations of the atomic displacements arising from irradiation and associated with nuclear losses of incident particles during interaction with ceramics, at irradiation fluences of 10^{14}–5×10^{15} cm^{-2} there are less than 0.01 dpa. Atomic displacements can have the main effect on deformation distortions at maximum irradiation fluences of 5×10^{16}–10^{17} cm^{-2}, for which the atomic displacements are more than 3–7 dpa. In that case, in conformity with the data of structural distortions, a marked rise in the crystal lattice deformation is observed, which can be not only due to the cumulative effect related to the ionization processes and changes in the electron density, but also to atomic displacements, which cause a rise in the deformation of the crystal structure. It is also worth noting that at maximum irradiation fluences, in conformity with the calculated data using the SRIM Pro 2013 program code, the concentration of implanted hydrogen in the damaged layers is more than 1 at.%, which can result in the formation of gas-filled regions resulting from deformation distortion of the ceramic crystal structure. The emergence of gas-filled cavities arising from the deformation distortion of the crystal lattice can result in structural embrittlement and softening of ceramics, since these areas are highly deformed inclusions that create additional distortions in the near-surface layer. The obtained data on structural changes and deformation distortions as a function of the dose of accumulated damage are in good agreement with a number of experimental works related to the study of structural distortions in oxide ceramics under irradiation with heavy ions [58–60]. Moreover, in contrast to irradiation with heavy ions, when it comes to proton irradiation, the accumulation of radiation damage proceeds much more slowly, which is not only due to the small size of protons, but also to differences in the ionization losses of incident particles during the interaction of protons with the crystal lattice. It should be noted that during proton irradiation, the thickness of the damaged layers is much greater, which can lead to large structural changes arising from irradiation. At the same time, the main structural distortions are associated with deformation mechanical stresses of tensile or

compressive type, both in the case of heavy ions [58–60] and irradiation with protons. Their accumulation results in the destruction of the damaged layers.

Figure 4 below demonstrates TEM images of the structural disorder of ceramics with a dopant concentration of 0.05 mol, before and after high-dose proton irradiation with a fluence of 10^{16} and 10^{17} cm^{-2}, reflecting the evolution of ceramic degradation with the formation of regions of disorder and the consequent emergence of gas-filled bubbles.
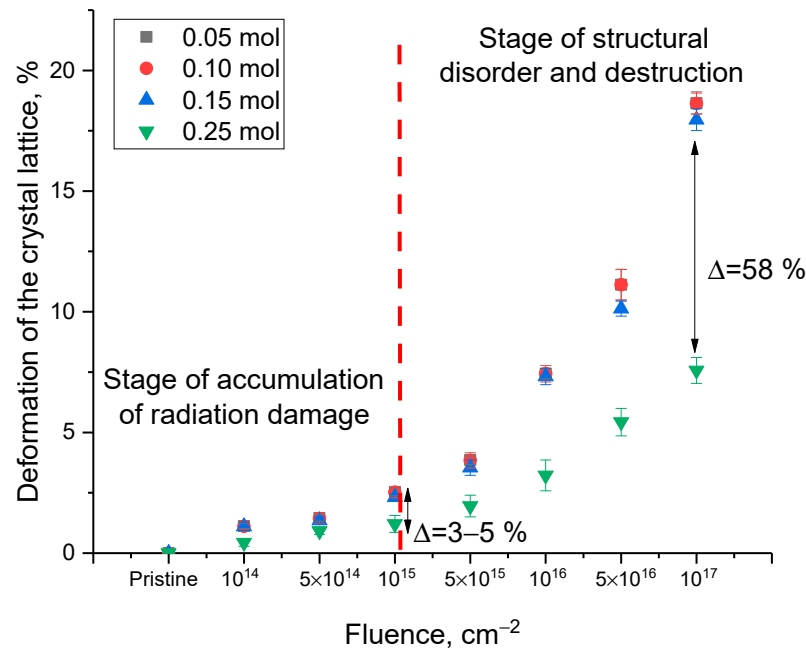

Figure 3. Results of evaluation of the degree of crystal lattice deformation as a function of the irradiation fluence.

The presented TEM images clearly demonstrate that after irradiation, the destruction of the crystal structure, disordering and partial amorphization are observed, which indicates a negative effect of irradiation on the features of ceramics. In the case of an irradiation fluence of 10^{17} cm^{-2}, the formation of a spherical inclusion typical of a gas-filled bubble is observed near the surface. Moreover, in conformity with the presented TEM images, these areas are agglomerated with each other, indicating their high mobility and the ability to unite. The shape of the bubbles, alongside the structural distortion formed around them, is in good agreement with the hypothesis put forward by Evans [61] about the mechanisms of formation of such inclusions. At the same time, for samples with a tetragonal type of crystal lattice, the formation of such inclusions in the near-surface layer was not found, which indicates a higher resistance of these ceramics to radiation-induced swelling and the formation of gas-filled bubbles.

Summarizing the observed structural changes associated with deformation distortions and their accumulation kinetics during irradiation, we can conclude the following: The main contribution to the structural disordering of ceramic samples is made by the cumulative effect of deformation tensile stresses capable of distorting the crystal structure, and at high irradiation fluences for ceramics with a monoclinic phase, the emergence of gas-filled bubbles. Moreover, the processes of polymorphic transformations during irradiation with protons were not observed even at irradiation fluences of 10^{16}–10^{17} cm^{-2}, which also confirms the previously stated assumption concerning the energy dependence of incident particles in the initialization of the polymorphic transformation processes in zirconium dioxide [40–42]. When it comes to the $Zr_{0.85}Ce_{0.15}O_2$ tetragonal phase formation under proton irradiation, an increased resistance to deformation distortions of the crystal structure is observed, which can be explained by structural effects, and by a more ordered structure of ceramics in the initial state.
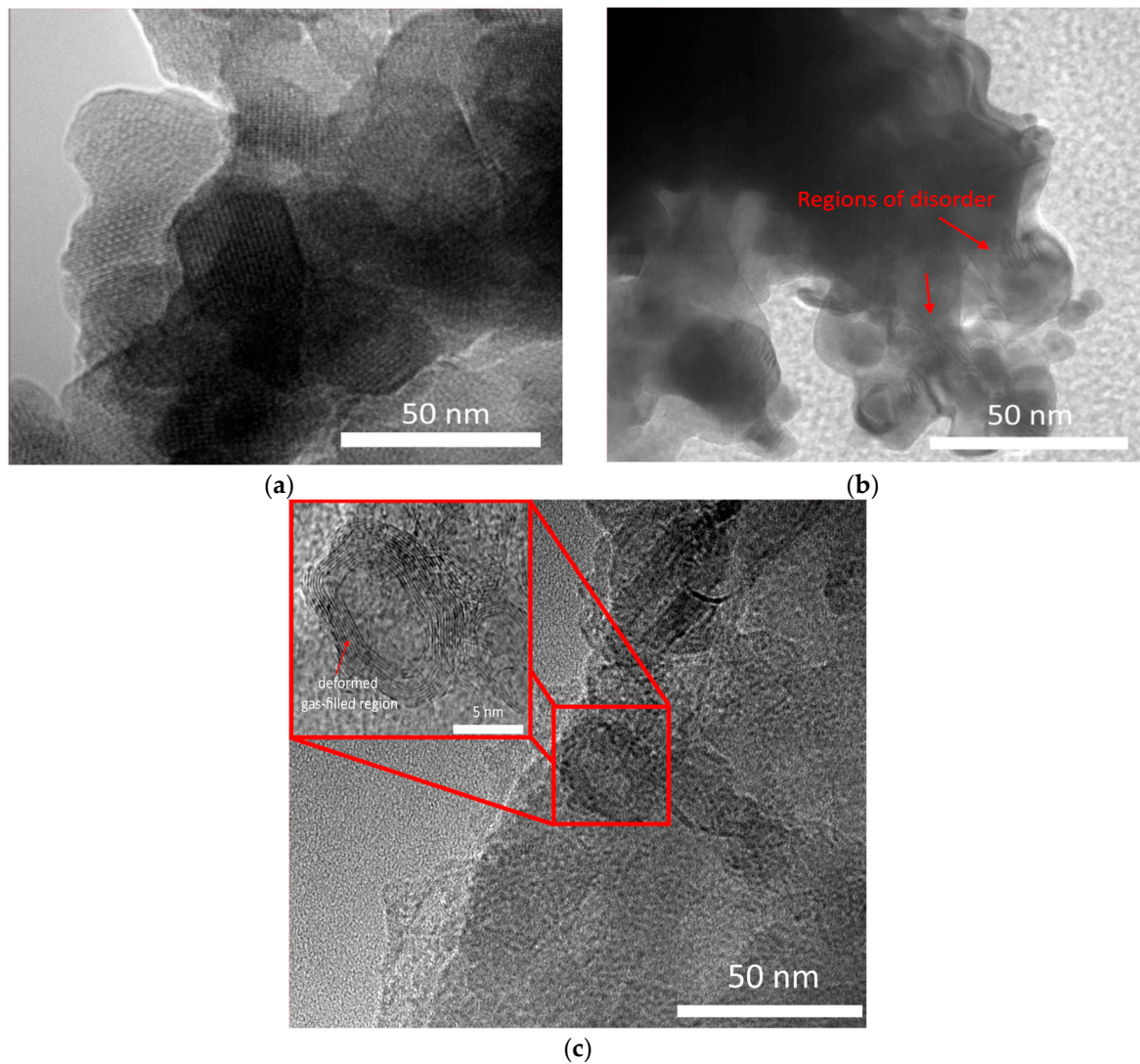
Figure 4. TEM images of ceramics with a dopant concentration of 0.05 mol before (**a**) and after high-dose proton irradiation with a fluences of 10^{16} cm^{-2} (**b**) and 10^{17} cm^{-2} (**c**).

3.3. Influence of Structural Distortions and Radiation Damage Accumulation on the Alteration in the Strength Properties of Ceramics

An important factor for establishing the criteria for the applicability of composite ceramics as inert matrix materials is the assessment of their strength properties, the change in which directly affects the stability of the fissile material since in the case of a sharp deterioration in strength, embrittlement of the insulating inert material that holds the fissile fuel can occur. In that case, there is a risk of contact of fissile material and the subsequent formation of areas with increased heat release, which can result in a destructive alteration in the entire fuel assembly.

Figure 5 shows the results of changes in the hardness of ceramics as a function of the irradiation fluence, reflecting the degree of structural softening as a result of accumulated structural distortions and deformation inclusions. When analyzing the obtained values of the hardness of the samples in the initial state as a function of the concentration of the CeO$_2$ dopant, it can be concluded that the alteration in the phase composition associated with the formation of the Zr$_{0.98}$Ce$_{0.02}$O$_2$ substitution phase results in a rise in hardness by 6% in comparison with the samples obtained at dopant concentrations of 0.05 mol. In the case of the formation of two-phase ceramics, the formation of which occurs at a dopant concentration of 0.10 mol, the increase in hardness is more than 36%, and for ceramics with the dominant tetragonal Zr$_{0.85}$Ce$_{0.15}$O$_2$ phase, the increase in hardness is more than three

times that of ceramics with the monoclinic ZrO_2 phase. Such an alteration in the strength characteristics indicates a rise in the resistance of ceramics to mechanical stress, alongside a growth in their resistance to external mechanical stress.
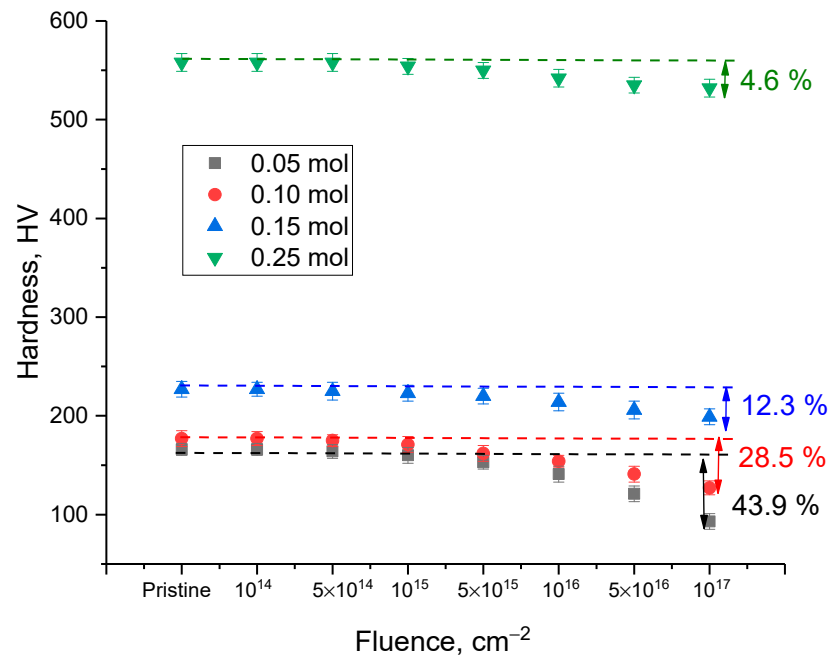

Figure 5. Results of changes in the strength characteristics of ceramics as a function of the irradiation fluence.

As is evident from the data proposed, the most pronounced alterations in the hardness of ceramics are observed at irradiation fluences above 10^{15} cm^{-2}, which is in good agreement with the results of changes in the deformation distortions of ceramics as a result of the cumulative effect. In that case, the change in hardness occurs only when the cumulative effect of deformation distortions results in a growth in structural disorder by more than 2–4%; at lower values of the alteration in the strength characteristics of ceramics, it has not been established. Moreover, in contrast to changes in the value of structural disorder and deformation distortions, the change in strength properties has a more pronounced dependence on changes in the phase composition of ceramics. Thus, in the case of the formation of a monoclinic $Zr_{0.98}Ce_{0.02}O_2$ substitution phase in the structure, the maximum decrease in hardness at the maximum irradiation fluence (10^{17} cm^{-2}) is no more than 28.5% of the initial value, while for the monoclinic ZrO_2 phase, a similar change is more than 43% of the initial value. In the case of the formation of a two-phase structure consisting of a mixture of the monoclinic and tetragonal phases, the maximum decrease in hardness at an irradiation fluence of 10^{17} cm^{-2} is no more than 12%, which is 3.5 times less than the corresponding value for single-phase ceramics with the ZrO_2 monoclinic phase. It should also be noted that for ceramics with the $Zr_{0.85}Ce_{0.15}O_2$ tetragonal phase, the maximum decrease in hardness at the maximum irradiation fluence is less than 5%, which indicates a high resistance to destructive softening of the samples. Such a difference in the strength characteristics and a growth in resistance to softening with an alteration in the phase composition of ceramics implies that the main contribution to maintaining the stability of strength properties is made by the phase composition of ceramics, which, as for polymorphic transformations of the monoclinic $Zr_{0.98}Ce_{0.02}O_2 \rightarrow$ tetragonal $Zr_{0.85}Ce_{0.15}O_2$ type, results in strengthening and a growth in stability. It should also be noted that a steep deterioration in the strength characteristics for ceramic samples with a low dopant concentration (0.05 mol) can also be due to the effects related to the formation of gas-filled inclusions in the near-surface layer, which, as a result of external mechanical influences, result in a destructive embrittlement and a major drop in resistance to cracking and crack formation.

Summarizing the above, it can be concluded that the results of the change in strength characteristics indicate that the alteration in the phase composition of ceramics with an increase in the CeO_2 dopant concentration results in a growth in the degree of destruction resistance when the radiation damage accumulates.

4. Conclusions

During the studies, it was revealed that a rise in the cerium dioxide dopant concentration from 0.05 to 0.15 mol does not result in significant alterations in the resistance of ceramics to radiation-induced embrittlement during swelling and subsequent destruction of the near-surface layer in the case of proton irradiation. When it comes to dopant concentrations of 0.20–0.25 mol, a growth in the resistance of ceramics to radiation-induced destruction under high-dose irradiation is observed. This behavior of stability can be due to the structural changes related to the formation of a substitutional solid solution and subsequent polymorphic transformation of the monoclinic $Zr_{0.98}Ce_{0.02}O_2 \rightarrow$ tetragonal $Zr_{0.85}Ce_{0.15}O_2$ type, alongside a growth in the dislocation density with a decrease in the grain size in doped ceramics. During conducted studies, it was found that the deformation distortion of the crystal structure is associated with the accumulation of radiation-induced tensile residual stresses, alongside implanted hydrogen during high-dose irradiation. In that case, a polymorphic transformation of the monoclinic $Zr_{0.98}Ce_{0.02}O_2 \rightarrow$ tetragonal $Zr_{0.85}Ce_{0.15}O_2$ type results in a rise in the resistance to deformation distortion of the crystal lattice by more than two to three times.

The main result of this work is the obtained dependences of alterations in structure and strength as a function of the accumulated radiation damage in the near-surface layers of ceramics, alongside the established connection between the influence of variations in the phase composition of ceramics on growing resistance to radiation embrittlement. Subsequently, the obtained results can be used in the design of a dispersed nuclear fuel, and in the determination of its applicability, when taking into account all of the data obtained.

Author Contributions: Conceptualization, M.V.Z., I.E.K., D.B.B. and A.L.K.; methodology, D.I.S., I.E.K., M.V.Z. and A.L.K.; formal analysis, M.V.Z., D.B.B. and A.L.K.; investigation, I.E.K., M.V.Z., D.I.S. and A.L.K.; resources, A.L.K.; writing—original draft preparation, review and editing, I.E.K., D.B.B. and A.L.K.; visualization, A.L.K.; supervision, A.L.K. All authors have read and agreed to the published version of the manuscript.

Data Availability Statement: Not applicable.

Conflicts of Interest: The authors declare no conflict of interest.

References

1. Capps, N.; Schappel, D.; Nelson, A. Initial development of an RIA envelope for dispersed nuclear fuel. *Ann. Nucl. Energy* **2020**, *148*, 107719. [CrossRef]
2. Ding, S.; Wang, Q.; Huo, Y. Mechanical behaviors of the dispersion nuclear fuel plates induced by fuel particle swelling and thermal effect II: Effects of variations of the fuel particle diameters. *J. Nucl. Mater.* **2010**, *397*, 80–91. [CrossRef]
3. Song, T.; Wang, Y.; Chang, Z.; Guo, L. In-situ fabrication of dispersion nuclear fuel pellets with a core-shell structure. *Ann. Nucl. Energy* **2019**, *134*, 258–262. [CrossRef]
4. Pillon, S.; Wallenius, J. Oxide and nitride TRU fuels: Lessons drawn from the CONFIRM and FUTURE projects of the 5th European Framework Program. *Nucl. Sci. Eng.* **2006**, *153*, 245–252. [CrossRef]
5. Frieß, F.; Liebert, W. Inert-matrix fuel for transmutation: Selected mid-and long-term effects on reprocessing, fuel fabrication and inventory sent to final disposal. *Prog. Nucl. Energy* **2022**, *145*, 104106. [CrossRef]
6. Saoudi, M.; Barry, A.; Lang, J.; Boyer, C.; Rogge, R.B.; Corbett, S.; Wang, X. Post-irradiation examination of U-7Mo/Mg and U-10Mo/Mg dispersion fuels irradiated in the NRU reactor. *J. Nucl. Mater.* **2022**, *558*, 153343. [CrossRef]

7. Terricabras, A.J.; Wang, L.; Raftery, A.M.; Nelson, A.T.; Zinkle, S.J. Properties and microstructure evolution of silicon nitride and zirconium nitride following Ni ion irradiation. *J. Nucl. Mater.* **2022**, *563*, 153643. [CrossRef]

8. Chen, J.; Liu, H.; Zhang, R.; Li, G.; Yi, D.; Lin, G.; Guo, Z.; Liu, S. High-temperature deformation and processing maps of Zr-4 metal matrix with dispersed coated surrogate nuclear fuel particles. *Results Phys.* **2018**, *9*, 1057–1066. [CrossRef]

9. Jiang, Y.; Wang, Q.; Cui, Y.; Huo, Y.; Ding, S. Simulation of irradiation hardening of Zircaloy within plate-type dispersion nuclear fuel elements. *J. Nucl. Mater.* **2011**, *413*, 76–89. [CrossRef]

10. Osaka, M.; Miwa, S.; Tachi, Y. Simple fabrication process for CeO_2–MgO composite as surrogate for actinide-containing target for use in nuclear fuel. *Ceram. Int.* **2006**, *32*, 659–663. [CrossRef]

11. Monge, M.A.; González, R.; Muñoz Santiuste, J.E.; Pareja, R.; Chen, Y.; Kotomin, E.A.; Popov, A.I. Photoconversion and dynamic hole recycling process in anion vacancies in neutron-irradiated MgO crystals. *Phys. Rev. B* **1999**, *60*, 3787–3791. [CrossRef]

12. Savoini, B.; Cáceres, D.; Vergara, I.; González, R.; Muñoz Santiuste, J.E. Radiation damage in neutron-irradiated yttria-stabilized-zirconia single crystals. *J. Nucl. Mater.* **2000**, *277*, 199–203. [CrossRef]

13. Konings, R.J.M.; Bakker, K.; Boshoven, J.G.; Conrad, R.; Hein, H. The influence of neutron irradiation on the microstructure of Al_2O_3, $MgAl_2O_4$, $Y_3Al_5O_{12}$ and CeO_2. *J. Nucl. Mater.* **1998**, *254*, 135–142. [CrossRef]

14. Monge, M.A.; Gonzalez, R.; Muñoz Santiuste, J.E.; Pareja, R.; Chen, Y.; Kotomin, E.A.; Popov, A.I. Photoconversion of F^+ centers in neutron-irradiated MgO. *Nucl. Instrum. Methods Phys. Res. Sect. B Beam Interact. Mater. At.* **2000**, *166*, 220–224. [CrossRef]

15. Ehrhart, P.; Averback, R.S.; Popov, A.I.; Sambeek, A.V. Defects in ion implanted and electron irradiated MgO and Al_2O_3. *Radiat. Eff. Defects Solids* **1995**, *136*, 169–173. [CrossRef]

16. Seeman, V.; Feldbach, E.; Kärner, T.; Maaroos, A.; Mironova-Ulmane, N.; Popov, A.I.; Shablonin, E.; Vasil'chenko, E.; Lushchik, A. Fast-neutron-induced and as-grown structural defects in magnesium aluminate spinel crystals with different stoichiometry. *Opt. Mater.* **2019**, *91*, 42–49. [CrossRef]

17. Lushchik, A.; Dolgov, S.; Feldbach, E.; Pareja, R.; Popov, A.I.; Shablonin, E.; Seeman, V. Creation and thermal annealing of structural defects in neutron-irradiated $MgAl_2O_4$ single crystals. *Nucl. Instrum. Methods Phys. Res. Sect. B Beam Interact. Mater. At.* **2018**, *435*, 31–37. [CrossRef]

18. Lee, Y.W.; Lee, S.C.; Kim, H.S.; Young, C.Y.; Degueldre, C. Study on the mechanical properties and thermal conductivity of silicon carbide-, zirconia-and magnesia aluminate-based simulated inert matrix nuclear fuel materials after cyclic thermal shock. *J. Nucl. Mater.* **2003**, *319*, 15–23. [CrossRef]

19. Kozlovskiy, A.L.; Zdorovets, M.V.; Shlimas, D.I. Study of the Morphological and Structural Features of Inert Matrices Based on ZrO_2–CeO_2 Doped with Y_2O_3 and the Effect of Grain Sizes on the Strength Properties of Ceramics. *Metals* **2022**, *12*, 1687. [CrossRef]

20. Angle, J.P.; Nelson, A.T.; Men, D.; Mecartney, M.L. Thermal measurements and computational simulations of three-phase (CeO_2–$MgAl_2O_4$–$CeMgAl_{11}O_{19}$) and four-phase (3Y-TZP–Al_2O_3–$MgAl_2O_4$–$LaPO_4$) composites as surrogate inert matrix nuclear fuel. *J. Nucl. Mater.* **2014**, *454*, 69–76. [CrossRef]

21. Yun, D.; Lu, C.; Zhou, Z.; Wu, Y.; Liu, W.; Guo, S.; Shi, T.; Stubbins, J.F. Current state and prospect on the development of advanced nuclear fuel system materials: A review. *Mater. Rep. Energy* **2021**, *1*, 100007. [CrossRef]

22. Meyer, M.K.; Hofman, G.L.; Hayes, S.L.; Clark, C.R.; Wiencek, T.C.; Snelgrove, J.L.; Strain, R.V.; Kim, K.-H. Low-temperature irradiation behavior of uranium–molybdenum alloy dispersion fuel. *J. Nucl. Mater.* **2002**, *304*, 221–236. [CrossRef]

23. Zhang, J.; Wang, H.; Wei, H.; Tang, C.; Lu, C.; Huang, C.; Ding, S.; Li, Y. Modelling of effective irradiation swelling for inert matrix fuels. *Nucl. Eng. Technol.* **2021**, *53*, 2616–2628. [CrossRef]

24. Zhao, Y.; Gong, X.; Ding, S.; Huo, Y. A numerical method for simulating the non-homogeneous irradiation effects in full-sized dispersion nuclear fuel plates. *Int. J. Mech. Sci.* **2014**, *81*, 174–183. [CrossRef]

25. Dong, Y.; Lv, J.; Zuo, H.; Li, Q. Explicit Analysis of Nonuniform Irradiation Swelling Pressure Exerting on Dispersion Fuel Matrix Based on the Equivalent Inclusion Method. *Materials* **2022**, *15*, 3231. [CrossRef]

26. Li, Y.; Wang, J.; Zhao, L.; Yao, C.; Li, P.; Huang, F.; Meng, F. Improved thermal stability and irradiation tolerance of oxide dispersion strengthened chromium coatings. *J. Nucl. Mater.* **2023**, *577*, 154328. [CrossRef]

27. Zhao, J.; Chen, Z.; Tu, J.; Zhao, Y.; Dong, Y. Application of LSTM Approach for Predicting the Fission Swelling Behavior within a CERCER Composite Fuel. *Energies* **2022**, *15*, 9053. [CrossRef]

28. Polovnikov, P.V.; Tarasov, V.I.; Veshchunov, M. Modelling of breakaway swelling in intermetallic fuels during low-temperature irradiation. *J. Nucl. Mater.* **2022**, *558*, 153362. [CrossRef]

29. Matzke, H. Radiation effects in nuclear fuels. In *Radiation Effects in Solids*; Sickafus, K.E., Kotomin, E.A., Uberuaga, B.P., Eds.; Springer: Dordrecht, The Netherlands, 2007; pp. 401–420. [CrossRef]

30. Castin, N.; Terentyev, D.; Bakaev, A.; Stankovskiy, A.; Bonny, G. On the equivalence of irradiation conditions on present and future facilities for fusion materials research and qualification: A computational study. *J. Nucl. Mater.* **2022**, *562*, 153589. [CrossRef]

31. Neto, I.; Roberto, R.; Kardoulaki, E.; Valdez, J.A. The influence of the processing parameters on the reactive flash sintering of ZrO_2-CeO_2. *J. Am. Ceram. Soc.* **2022**, *105*, 3937–3948. [CrossRef]

32. Giniyatova, S.G.; Sailaukhanov, N.A.; Nesterov, E.; Zdorovets, M.V.; Kozlovskiy, A.L.; Shlimas, D.I. Research of Structural, Strength and Thermal Properties of ZrO_2—CeO_2 Ceramics Doped with Yttrium. *Crystals* **2022**, *12*, 242. [CrossRef]

33. Koike, M.; Kodaira, A.; Tokunaga, T.; Yamamoto, T. Shrinkage-rate controlled flash sintering for 3–10 mol% Y_2O_3-doped ZrO_2 polycrystals. *J. Ceram. Soc. Jpn.* **2022**, *130*, 906–912. [CrossRef]

34. Clark, D.; Zinkle, S.; Patel, M.; Parish, C. High temperature ion irradiation effects in MAX phase ceramics. *Acta Mater.* **2016**, *105*, 130–146. [CrossRef]

35. Casalegno, V.; Kondo, S.; Hinoki, T.; Salvo, M.; Czyrska-Filemonowicz, A.; Moskalewicz, T.; Katoh, Y.; Ferraris, M. $CaO-Al_2O_3$ glass-ceramic as a joining material for SiC based components: A microstructural study of the effect of Si-ion irradiation. *J. Nucl. Mater.* **2018**, *501*, 172–180. [CrossRef]

36. Zhumazhanova, A.; Mutali, A.; Ibrayeva, A.; Skuratov, V.; Dauletbekova, A.; Korneeva, E.; Akilbekov, A.; Zdorovets, M. Raman Study of Polycrystalline Si_3N_4 Irradiated with Swift Heavy Ions. *Crystals* **2021**, *11*, 1313. [CrossRef]

37. van Vuuren, A.J.; Ibrayeva, A.D.; Skuratov, V.A.; Zdorovets, M.V. Analysis of the microstructural evolution of silicon nitride irradiated with swift Xe ions. *Ceram. Int.* **2020**, *46*, 7155–7160. [CrossRef]

38. Thomé, L.; Moll, S.; Sattonnay, G.; Vincent, L.; Garrido, F.; Jagielski, J. Radiation effects in cubic zirconia: A model system for ceramic oxides. *J. Nucl. Mater.* **2009**, *389*, 297–302. [CrossRef]

39. Florez, R.; Crespillo, M.L.; He, X.; White, T.A.; Hilmas, G.; Fahrenholtz, W.; Graham, J. The irradiation response of ZrC ceramics under 10 MeV Au^{3+} ion irradiation at 800 °C. *J. Eur. Ceram. Soc.* **2020**, *40*, 1791–1800. [CrossRef]

40. Beck, H.; Kaliba, C. On the solubility of Fe, Cr and Nb in ZrO_2 and its effect on thermal dilatation and polymorphic transition. *Mater. Res. Bull.* **1990**, *25*, 1161–1168. [CrossRef]

41. Manik, S.K.; Dutta, H.; Pradhan, S.K. Microstructure characterization and phase transformation kinetics of polymorphic transformed ball milled a-TiO_2–10 mol% m-ZrO_2 mixture by Rietveld method. *Mater. Chem. Phys.* **2003**, *82*, 848–859. [CrossRef]

42. Dippel, A.-C.; Jensen, K.M.; Tyrsted, C.; Bremholm, M.; Bøjesen, E.D.; Saha, D.; Birgisson, S.; Christensen, M.; Billinge, S.J.L.; Iversen, B.B. Towards atomistic understanding of polymorphism in the solvothermal synthesis of ZrO_2 nanoparticles. *Acta Crystallogr. Sect. A Found. Adv.* **2016**, *72*, 645–650. [CrossRef]

43. Yashima, M.; Takashina, H.; Kakihana, M.; Yoshimura, M. Low-Temperature Phase Equilibria by the Flux Method and the Metastable–Stable Phase Diagram in the ZrO_2–CeO_2 System. *J. Am. Ceram. Soc.* **1994**, *77*, 1869–1874. [CrossRef]

44. Li, L.; Van Der Biest, O.; Wang, P.L.; Vleugels, J.; Chen, W.W.; Huang, S.G. Estimation of the phase diagram for the ZrO_2–Y_2O_3–CeO_2 system. *J. Eur. Ceram. Soc.* **2001**, *21*, 2903–2910. [CrossRef]

45. Li, J.; Peng, J.; Guo, S.; Qv, W.; Chen, G.; Li, W.; Zhang, L. Martensitic transformation thermodynamic calculation of ZrO_2–MgO system. *Phase Transit.* **2012**, *85*, 1022–1029. [CrossRef]

46. Wen, T.; Yuan, L.; Tian, C.; Yan, Z.; Liu, Z.; Yu, J. Electrical conductivity behavior of ZrO_2-MgO-Y_2O_3 ceramic: Effect of heat treatment temperature. *J. Aust. Ceram. Soc.* **2022**, *58*, 421–427. [CrossRef]

47. Li, J.; Peng, J.; Guo, S.; Qv, W.; Li, W.; Zhang, L.; Chen, G. Thermodynamic calculations of t to m martenstic transformation of ZrO_2–CaO binary system. *Ceram. Int.* **2012**, *38*, 2743–2747. [CrossRef]

48. Bruni, Y.L.; Garrido, L.B.; Aglietti, E.F. Properties of $CaO-ZrO_2$ Based Composites. *Procedia Mater. Sci.* **2015**, *8*, 203–210. [CrossRef]

49. Neetu; Singh, D.; Kumar, N.; Gangwar, J. Comparative study of crystallographic representation on the three ZrO_2 polymorphs: Structural models, lattice planes, model electron and nuclear densities. *Mater. Res. Express* **2019**, *6*, 1150f8. [CrossRef]

50. Kurakhmedov, A.E.; Morzabayev, A.K.; Tleubay, I.; Berguzinov, A.; Kozlovskiy, A.L. Study of the Mechanisms of Polymorphic Transformations in Zirconium Dioxide upon Doping with Magnesium Oxide, as Well as Establishing the Relationship between Structural Changes and Strength Properties. *Ceramics* **2023**, *6*, 1164–1178. [CrossRef]

51. Schwartz, K.; Volkov, A.E.; Sorokin, M.V.; Trautmann, C.; Voss, K.-O.; Neumann, R.; Lang, M. Effect of electronic energy loss and irradiation temperature on color-center creation in LiF and NaCl crystals irradiated with swift heavy ions. *Phys. Rev. B* **2008**, *78*, 024120. [CrossRef]

52. Medvedev, N.A.; Rymzhanov, R.A.; Volkov, A.E. Time-resolved electron kinetics in swift heavy ion irradiated solids. *J. Phys. D Appl. Phys.* **2015**, *48*, 355303. [CrossRef]

53. Luo, P.; Sun, X.Y.; Li, Y.; Yang, L.; Shao, W.Z.; Zhen, L.; Xu, C.Y. Correlation between Structural Evolution and Device Performance of $CH_3NH_3PbI_3$ Solar Cells under Proton Irradiation. *ACS Appl. Energy Mater.* **2021**, *4*, 13504–13515. [CrossRef]

54. Reali, L.; Boleininger, M.; Gilbert, M.R.; Dudarev, S.L. Macroscopic elastic stress and strain produced by irradiation. *Nucl. Fusion* **2022**, *62*, 016002. [CrossRef]

55. Alin, M.; Kozlovskiy, A.L.; Zdorovets, M.V.; Uglov, V.V. Study of the mechanisms of the t-ZrO_2→c-ZrO_2 type polymorphic transformations in ceramics as a result of irradiation with heavy Xe^{22+} ions. *Solid State Sci.* **2022**, *123*, 106791. [CrossRef]

56. Kozlovskiy, A.L.; Alin, M.; Borgekov, D.B. Study of Polymorphic Transformation Processes and Their Influence in Polycrystalline ZrO_2 Ceramics upon Irradiation with Heavy Ions. *Ceramics* **2023**, *6*, 686–706. [CrossRef]

57. Ghyngazov, S.A.; Boltueva, V.A.; O'Connell, J.H.; Vershinina, T.N.; Kirilkin, N.S.; Rymzhanov, R.A.; Skuratov, V.A.; Surzhikov, A.P. Swift heavy ion induced phase transformations in partially stabilized ZrO_2. *Radiat. Phys. Chem.* **2022**, *192*, 109917. [CrossRef]

58. Palomares, R.I.; Shamblin, J.; Tracy, C.L.; Neuefeind, J.; Ewing, R.C.; Trautmann, C.; Lang, M. Defect accumulation in swift heavy ion-irradiated CeO_2 and ThO_2. *J. Mater. Chem. A* **2017**, *5*, 12193–12201. [CrossRef]

59. Cureton, W.F.; Palomares, R.I.; Walters, J.; Tracy, C.L.; Chen, C.-H.; Ewing, R.C.; Baldinozzi, G.; Lian, J.; Trautmann, C.; Lang, M. Grain size effects on irradiated CeO_2, ThO_2, and UO_2. *Acta Mater.* **2018**, *160*, 47–56. [CrossRef]

60. Cureton, W.F.; Tracy, C.L.; Lang, M. Review of swift heavy ion irradiation effects in CeO$_2$. *Quantum Beam Sci.* **2021**, *5*, 19. [CrossRef]

61. Evans, T.; Norris, S. Swelling as a stabilizing mechanism in irradiated thin films: II. Effect of swelling rate. *J. Phys. Condens. Matter* **2022**, *34*, 325302. [CrossRef]